

PLANETARY MOON CYCLER TRAJECTORIES^{*}

Ryan P. Russell[†] and Nathan J. Strange[‡]

Free-return cycler trajectories repeatedly shuttle a spacecraft between two bodies using little or no fuel. Here, the cycler architecture is proposed as a complementary and alternative method for designing planetary moon tours. Previously applied enumerative cycler search and optimization techniques are generalized and specifically implemented in the Jovian and Saturnian moon systems. In addition, the algorithms are tested for general use to find non-Earth heliocentric cyclers. Overall, hundreds of ideal model ballistic cycler geometries are found and several representative cases are documented and discussed. Many of the ideal model solutions are found to remain ballistic in a zero radius sphere of influence patched conic ephemeris model, and preliminary work in a high-fidelity fully integrated model demonstrates near-ballistic cycles for several example cases. In the context of recent Cassini discoveries, the Saturn-Titan-Enceladus system is investigated in the most detail and many promising solutions result. Several of the high energy Titan-Enceladus cyclers find immediate application as Cassini extended missions options that provide frequent low altitude Enceladus flybys.

INTRODUCTION

Cyclor orbits offer a low propellant cost means for the exploration of multiple high interest moons such as the Galilean moons at Jupiter, Titan, and the icy moons at Saturn. The Galilean moons have long been a top priority for space exploration. Europa, Ganymede, and Callisto each are speculated to support large subsurface liquid water oceans, and the proximity to the surface and the size of Europa's ocean has compelling astrobiological implications that makes Europa the top priority of destinations on NASA's Solar System Exploration Roadmap[§]. Io is extremely active volcanically and has a young surface, and Ganymede is the only moon in the solar system known to have a magnetic field. At Saturn, Titan is one of the most Earth-like bodies in the solar system because of its complex atmosphere, methane hydrological cycle, dynamic surface, and organic signatures. Enceladus has recently become a high priority target because Cassini identified ice crystal plumes that may originate from a liquid source extremely close to the surface.

Traditionally, cycler orbit theory has been applied to the Sun-Earth-Mars system for application to human missions [1-13]. Earth-Mars cycler applications generally suffer from long repeat periods, infrequent launch opportunities, and the risky requirement to perform hyperbolic rendezvous [14]. In contrast, the brief synodic periods of most planetary moon pairs lead to an abundance of cycler solutions with short repeat periods and frequent initiation opportunities. Further, the mission objectives of a planetary moon cycler are achieved en route and during flybys only and therefore do not require hyperbolic rendezvous.

In this study cycler search techniques previously applied to the Earth-Mars case are expanded to seek similar repeating trajectories between moons that orbit a common planet. The generalized cycler search algorithm provides timetables for the moon tour design space through an automated global search that finds and catalogues cycler opportunities. The cycler solutions identify feasible multi-body flyby resonances useful as stand-alone designs or preliminary guesses for sequences of conventional planetary tour designs. The cycler trajectories can provide critical reconnaissance and communication for planned orbiters, surface landers, and aerial vehicles while the repeat flybys enable remote sensing and in situ science of the multiple high priority targets.

The first sections overview the existing cycler search and optimization algorithms, describe the improvements and generalizations, and discuss the relevant moon systems and dynamical models. Next, the

^{*} Presented at the AAS/AIAA Space Flight Mechanics Meeting in Sedona, Arizona, Jan 29-Feb 1, 2007

[†] Jet Propulsion Laboratory, 4800 Oak Grove Drive, M/S 301-121, Pasadena, California 91109. Ryan.Russell@jpl.nasa.gov

[‡] Jet Propulsion Laboratory, 4800 Oak Grove Drive, M/S 230-205, Pasadena, California 91109. Nathan.Strange@jpl.nasa.gov

[§] http://solarsystem.nasa.gov/multimedia/downloads/SSE_RoadMap_2006_Report_FC-A_med.pdf [cited 11-30-06]

automated ideal (circular-coplanar) model search is applied to find cyclers for five Jovian moon pairs and the Titan-Enceladus pair in the Saturn system. Special attention is paid to Titan and Enceladus because Cassini discoveries have recently thrust both moons into the science spotlight. The generalized algorithms are also tested and verified in the heliocentric system and several potentially useful Venus-Mars and Venus-Mercury cyclers are examined. Each ideal model search results in hundreds of ballistic solutions. The solutions and characteristics are archived and a select few of the best cases are documented and discussed. Several of the solutions are optimized over multiple periods in a zero radius sphere of influence patched conic ephemeris model and remain ballistic. Of the most promising solutions is the Titan-Enceladus Cycler#235 that includes 9 targeted Enceladus encounters, 45 targeted Titan encounters, full orbit rotation around Saturn (for complete lighting conditions), and near Hohmann velocities at Enceladus during a 2.4 year flight time. Several of the higher energy Titan-Enceladus cyclers have potential applications for Cassini extended missions. Finally, to demonstrate the transition from the patched conic ephemeris model to a high-fidelity model, multiple legs of a select few cyclers are optimized in a fully integrated n -body plus oblateness model.

APPROACH

The general cycler trajectory problem is to find an indefinitely repeatable pattern of ballistic trajectories that cycle a spacecraft between two celestial bodies that orbit a common body. The repeatability requirement makes the problem substantially more difficult than typical intermoon or interplanetary spacecraft tours. In general, exactly repeatable cyclers only exist in simplified models. Therefore, the approach for solving the general cycler problem is reduced to two steps:

- 1) Perform a broad search for true cyclers in an ideal model consisting of circular and coplanar celestial body orbits. These ideal model cyclers are exactly periodic.
- 2) Evaluate and optimize multiple cycles of ideal model cyclers in more realistic models. Because the geometry of the realistic solar system model is not exactly periodic, each cycle of a realistic cycler will be quasi-periodic. In this study, two levels of fidelity are considered for realistic models: (a) Zero radius sphere of influence patched conic ephemeris model, and (b) Fully integrated n -body plus oblateness model.

To reduce the search space to a manageable size, a sub-set of cyclers called free-return cyclers are sought where one of the two orbiting celestial bodies in the ideal model is considered massless. For the case of the Sun-Earth-Mars system, the free-return cyclers in ideal and more realistic models are computed and analyzed in detail in [1-12]. The current study generalizes the methods outlined in [7,9] to find free-return cyclers between any two celestial bodies that orbit a common body with near-circular, near-coplanar orbits. A brief overview of the method follows.

First, two bodies of interest are identified that have near-circular, near-coplanar orbits around a common body. Next, the magnitude of the spacecraft hyperbolic excess velocity (v_∞) with respect to the flyby body is chosen. Assuming the ideal circular-coplanar model, all direct free-return trajectories are calculated with the specified v_∞ that leave the flyby body and return ballistically within a specified maximum flight time. This procedure is described in detail in [6]. The solutions are easily visualized as a set of points and lines on the v_∞ globe as the example in Figure 1 illustrates. The vertical arrow represents the body velocity vector and the v_∞ globe is the locus of the tips of all possible v_∞ vectors that emanate from the tip of the body velocity vector. The z direction is aligned with the body velocity and the x direction is aligned with the body position with respect to the primary leaving the y direction to be orthogonal to the body orbit plane.

In Figure 1, solutions that return to the body after exactly an integer number of body revolutions around the primary exist as circles on the surface of the globe and are labeled “full-rev circles.” These types of free-returns are commonly referred to as resonant transfers. Solutions that return to the body after exactly an even integer number of half-body revolutions around the primary exist as points on the surface of the globe. They appear as above- and below-orbit plane pairs and are labeled “half-rev x’s” and “half-rev o’s” respectively. Lastly all free-return solutions with transfer angles that are not integer numbers of half-body revolutions exist as single points labeled “generic dots” and are constrained to the spacecraft orbit plane.

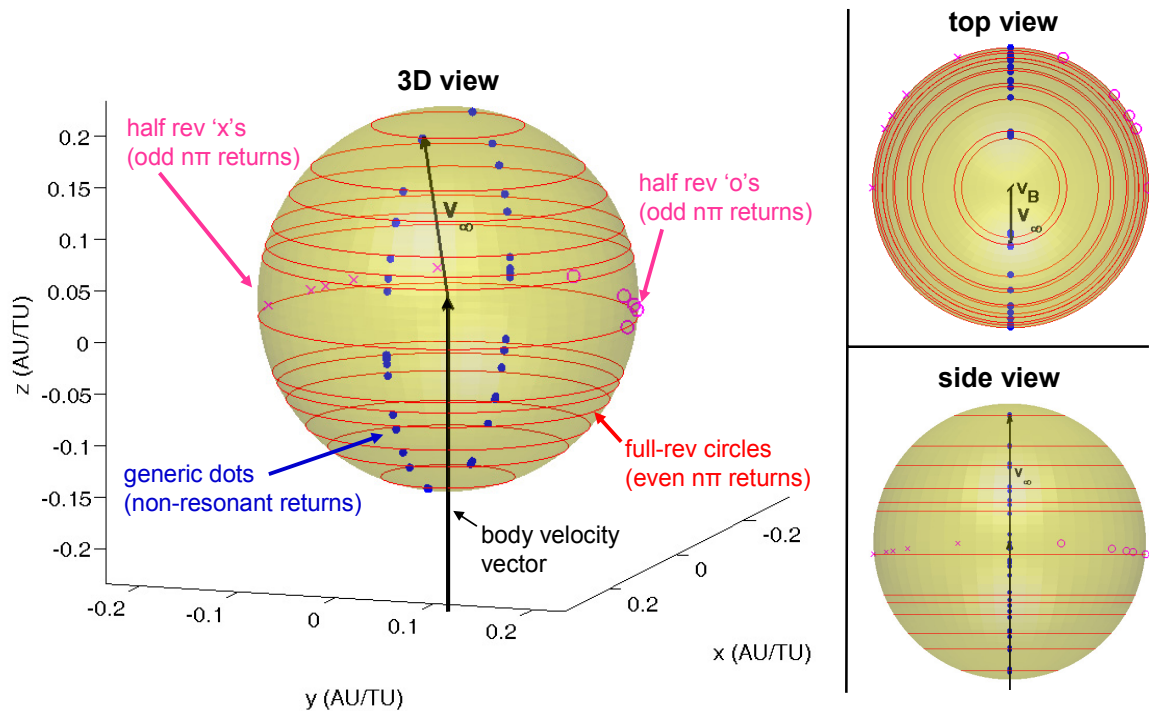


Figure 1: Example v_∞ globe identifying all three types of possible free-return solutions: half-revolution (odd $n\pi$ transfer angle), full-revolution (even $n\pi$), and generic (non- $n\pi$)

Gravity-assisted flybys provide a mechanism to connect multiple free-return trajectories. The flyby has the effect of rotating an incoming v_∞ vector by an angle whose magnitude is a function of the flyby altitude and the flyby body mass. In the circular coplanar model, the incoming and outgoing v_∞ magnitudes for all free-return trajectories are always identical. Therefore, a tour of free-return trajectories patched by gravity-assisted flybys can be constructed as discrete steps on the v_∞ globe where each step represents a rotation of the v_∞ vector. The maximum size of each step is limited by the turn angle associated with a flyby of a specified minimum altitude. The free-return cyclers problem is then reduced to a combinatorics problem of finding repeatable patterns that step the v_∞ vector from free-return solution to free-return solution. More specifically we want to find all 1-leg, 2-leg, ..., n -leg patterns that require valid flybys to navigate the v_∞ vector around the v_∞ globe on free-return solutions with a total combined flight time that is an integer multiple of the synodic period of the two bodies of interest. If at least one of the free-return solutions includes a trajectory that crosses the path of the second body of interest, then the pattern can be initiated such that an encounter occurs every period. Enumerating all of the possible combinations of half-revolution, full-revolution, and generic returns is well documented in Ref. [7]. The process is repeated for a full range of v_∞ values and results in a list of exactly periodic cyclers in the ideal model with a variety of defining characteristics.

For evaluation in a more realistic model, the ideal model solutions are propagated for several repeat cycles in the ideal model and a homotopy method is employed to parametrically walk the solution to a zero radius patched conic model that considers ephemeris locations of the bodies and models flybys as instantaneous body-centered velocity rotations. A final trajectory of up to ~ 50 legs is sought that is ballistic in the patched conic ephemeris model. This highly constrained trajectory optimization problem is described in detail in Ref. [9].

Finally, the resulting solutions are used as initial guesses for optimization in a high-fidelity force model including integrated flybys, n -body perturbations, and central-body oblateness. The high-fidelity optimization is performed with Mystic, a general-use software tool under development at the Jet Propulsion Laboratory [15]. Improving strategies for transitioning from the low- to the high-fidelity ephemeris solutions is an ongoing topic of research and warrants detailed future study. Here, it is emphasized that the high-fidelity optimization is included only to demonstrate reasonable Δv costs associated with realistic planetary moon cyclers.

Figure 2 illustrates an example of a cycler trajectory. A complete cycle is shown in detail of one of the most promising ideal model cyclers found in this study. The cycler begins at Titan on the ‘A’ label and performs a free-return to ‘B’ after 1.88 revs. A gravity-assist flyby places the cycler on a 1.23 rev free-return to ‘C’ and is followed by a 2:3 and consecutive 1:2 resonant returns to complete the cycle. The targeted Enceladus encounter occurs at ‘E’ in the middle of the fourth leg or the first 1:2 resonant free return. Each gravity-assisted flyby at Titan, including the flyby required to patch consecutive cycles, is well above the minimum altitude of 1000 km (the lowest flyby is 1843 km), making the cycler ballistic in the ideal model.

One Complete Cycle

- Leg 1 (A→B): Titan-Titan 1.88 revs
- Leg 2 (B→C): Titan-Titan 1.23 revs
- Leg 3 (C→D): Titan-Titan 2:3 resonance* (2 Titan revs, 3 sc revs)
- Leg 4 (D→E and E→F): Titan-Titan 1:2 resonance with intermediate Enceladus encounter after 1+ revs
- Leg 5 (F→G): Titan-Titan 1:2 resonance* (pictured out of plane)

*out of plane crank angle is degree of freedom

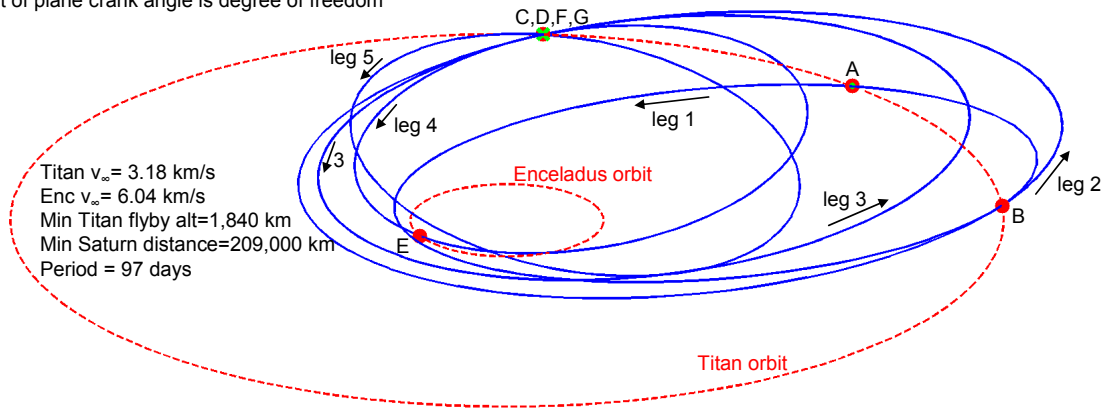


Figure 2: Three-dimensional diagram of one cycle of the ideal model Titan-Enceladus Cycler#235

IMPROVED CYCLER SEARCH CAPABILITIES

The search and optimization techniques from [7] and [9] are generalized to deal robustly with the vastly different time and distance scales associated with interplanetary and intermoon cyclers, including the ability for the flyby body to be inside or outside the orbit of the target body. The following subsections highlight the most important capabilities enabled by the current study.

Non-resonant free-return calculation

Given a specified v_∞ and M_{\max} where M is the floor of the number of flyby body revolutions, an algorithm is sought that provides all existing non-resonant return trajectories (or generic dots from Figure 1). The approach from [6] is based on a computationally expensive table look-up method while the new approach relies on a one dimensional root solving procedure and requires less memory storage and computational effort [16]. Figure 3 shows the period vs. flight time and v_∞ for all direct non-resonant free returns to a body in a circular orbit with $M \leq 3$ calculated from the multiple revolution Lambert problem [17,18,19]. It is emphasized that both the long and short period direct solutions from the classical Lagrange formulation of the Lambert problem [17,18] are reported in Figure 3. However, the inbound vs. outbound specification indicates the sign of the initial flight path angle and is unrelated to the short vs. long period specification. The objective is to obtain an algorithm that finds all intersections of a horizontal line of constant v_∞ with the solution curves from the lower half of Figure 3 (for arbitrary v_∞ and M_{\max}).

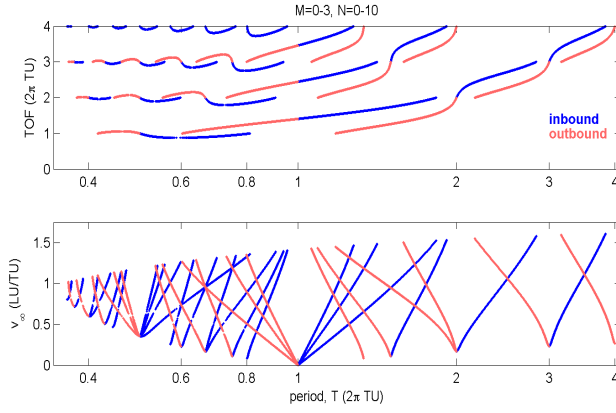


Figure 3: All direct non-resonant free returns to a body in circular orbit for $M \leq 3$

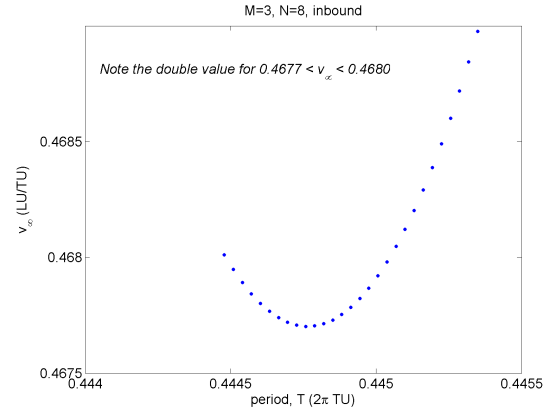


Figure 4: Zoomed view of Figure 3

Figure 5 gives an algorithm that reduces the problem to a one dimensional root-solving problem that requires iteration on the period, T , of the transfer ellipse. Note that all equations are normalized such that the circular radius of the flyby body is one length unit (LU) and the gravitational parameter of the primary is unity. The algorithm is restricted to elliptical direct orbits and therefore $0 < v_\infty < 1 + v_{\text{escape}}$ (where 1 is the velocity magnitude of the flyby body and $v_{\text{escape}} = 2^{1/2}$).

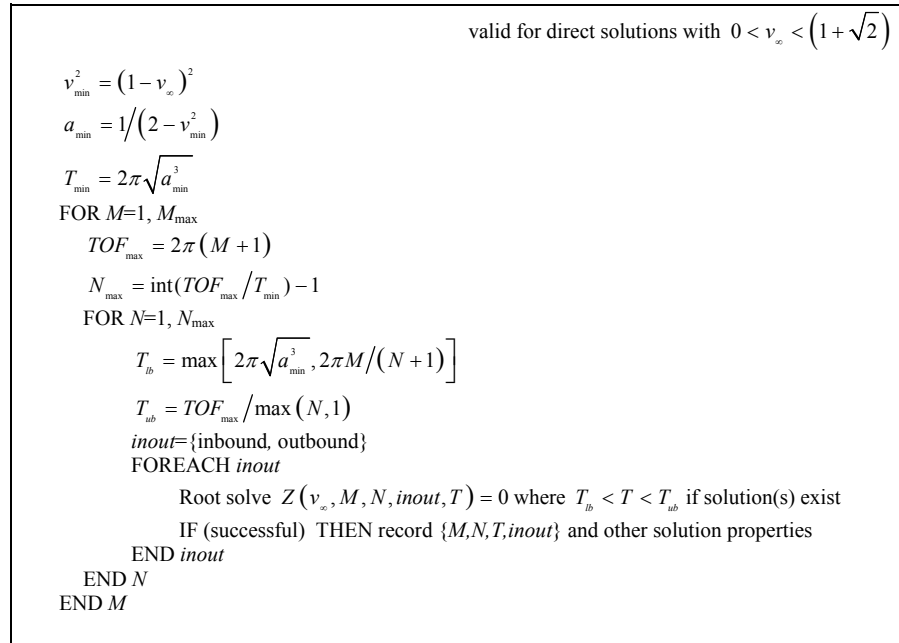


Figure 5: Algorithm for calculating all non-resonant returns with a specified v_∞ and maximum flight time

From Figure 1 the spacecraft velocity, v , after the flyby is minimized when the v_∞ vector is aligned opposite to the body velocity. The second line of the algorithm in Figure 5 calculates the minimum transfer semi-major axis, a_{\min} , from the conic equation and the minimum period follows on the third line. The maximum transfer flight time, TOF_{\max} , is calculated noting that one normalized flyby body period is 2π time units (TU). For a given M , the maximum floor of the number of transfer revolutions (N_{\max}) is calculated assuming the smallest possible transfer period and the largest possible flight time. For a given M and N , lower and upper bounds on the

transfer period guess are derived from inspection for direct transfers and expressed as T_{lb} and T_{ub} respectively. Next, T is iterated to seek solutions to the equation, $Z=0$, for both inbound and outbound transfers. If a solution exists, then $T_{lb} < T < T_{ub}$.

The highly nonlinear equation for Z is calculated as follows. Equations (1) and (2) give the transfer semi-major axis and departure velocity from two-body dynamics.

$$a = [T/(2\pi)]^{2/3} \quad (1)$$

$$v = \sqrt{2 - 1/a} \quad (2)$$

Equation (3) then provides the transfer eccentricity as a function of v_∞ . This expression is related to Tisserand's condition and details of the derivation are found in [16].

$$e = \sqrt{1 - (v^2 + 1 - v_\infty^2)^2 / (4a)} \quad (3)$$

Equation (4) gives the absolute value of the departure true anomaly from the conic equation and Eq. (5) expresses this as eccentric anomaly.

$$\nu = \left| \cos^{-1} \left[(a - ae^2 - 1) / e \right] \right| \quad (4)$$

$$E = \tan^{-1} \left[2 \tan(\nu/2) \sqrt{(1-e)/(1+e)} \right] \quad (5)$$

The short time to periapse then is

$$t_p = [E - e \sin(e)] / (2\pi/T) \quad (6)$$

Finally, $Z(M, N, v_\infty, inout)$ is expressed in Eq. (7) as the difference between the flight times of the spacecraft and the flyby body. For further details, see [16].

$$Z = \begin{cases} [T N + 2t_p] - [2\pi(M + \nu/\pi)] & \text{if } inout = \text{inbound} \\ [T(N+1) - 2t_p] - [2\pi(M + 1 - \nu/\pi)] & \text{if } inout = \text{outbound} \end{cases} \quad (7)$$

Over the valid range of $T_{lb} < T < T_{ub}$, Z is imaginary in some regions and suffers from multiple sign changes in the first and second derivatives with respect to T . One solution method for solving $Z(T)=0$ is to march through the valid range of T and initiate a gradient based root-solver when Z is real and a sign change is detected. Note that a few rare cases are observed where Z has two roots for fixed M, N , and $inout$. (See the double valued v_∞ in Figure 4.) However, from observation, the double valued solutions are near the impractical eccentricity of 1. An example application of the algorithm finds 220 non-resonant direct free-returns with $v_\infty = 0.5$ LU/TU when considering $M \leq 9$.

For the case of Titan as the flyby body, all non-resonant retrograde transfers with $v_\infty < 1.5$ LU/TU have periapse smaller than the radius of the outermost obstructive rings at 2.92 Saturn radii. If the resonant inclined orbits are considered, a few non-impact retrograde orbits begin to exist for $v_\infty > 1.12$ LU/TU. Note that the end of mission Cassini v_∞ is expected to be ~ 1.1 LU/TU. It is therefore not restrictive to ignore retrograde solutions for a cyclers Cassini extended mission. While it is possible to construct cyclers with retrograde orbits, it is generally not beneficial because the large v_∞ values reduce the available flyby bending angles and thus require prohibitively long cycle repeat periods. Despite its impracticality for the current application, to modify the algorithm in Figure 5 to account for retrograde orbits, the adjustments in Eqs. (8) and (9) are necessary. To implement, the $N=0$ case would require special attention to account for the near parabolic outbound solution with no upper bound on the period.

$$N_{\max} = \text{int}(TOF_{\max} / T_{\min}) \quad (8)$$

$$T_{ub} = \begin{cases} \infty & \text{if } N = 0 \\ 2\pi(M+2)/N & \text{if } N > 0 \end{cases} \quad (9)$$

Transitioning ideal model solutions to a patched conic ephemeris model

An improved approach for the homotopy method is implemented to parametrically “walk” an ideal model solution into a multiple cycle solution in a more realistic model. A previous approach [9] relies on the mean orbital elements of the orbiting celestial bodies where successive sub-problems are solved by slowly increasing the eccentricities and inclinations from circular-coplanar values to the true values, and the last sub-problem is solved using ephemeris body locations. The technique works well in the case of planets such as Earth and Mars where reality is closely modeled by Keplerian motion. However, the method struggles in the case of planetary moons where perturbations from other moons and central-body oblateness cause the motion to be poorly predicted using mean orbital elements.

The new approach parametrically walks the solution from the patched conic ideal model to a patched conic ephemeris model using several sub-problems where the location of the orbiting bodies are determined by a linear interpolation between the ideal model and ephemeris locations. Thus, for successive sub-problems, the model slowly morphs from a circular coplanar model into an ephemeris model. The approach is robust and easy to implement because it does not rely on user supplied mean elements for either body.

MODELS

The generalized free-return cypher search is applied to each of the ideal model systems in Table 1 where the primary is considered inertially fixed and the flyby and target bodies are in circular-coplanar orbits around the primary.

Table 1: Ideal models considered

Primary	Free-return flyby body	Target body
Sun	Earth	Mars
Sun	Venus	Mercury
Sun	Venus	Mars
Jupiter	Ganymede	Io
Jupiter	Ganymede	Europa
Jupiter	Ganymede	Callisto
Jupiter	Europa	Ganymede
Saturn	Titan	Enceladus

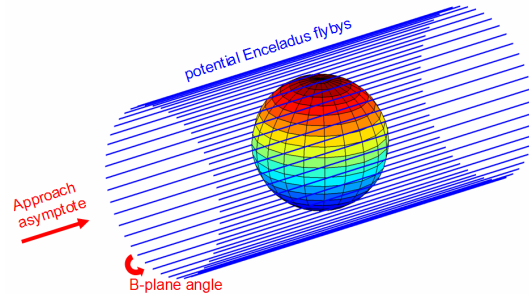


Figure 6: Flyby geometry at Enceladus

The Sun-Earth-Mars case is used to test and calibrate the improved methods noting that solutions to this system are well documented in [7,9]. The Sun-Venus-Mercury case is investigated as a mechanism to achieve multiple encounters with the two infrequently visited inner planets. The Sun-Venus-Mars case is evaluated in response to a recent study suggesting Venus-Mars cyclers as an alternative architecture to transport crew and cargo to Mars [20]. Further, the heliocentric cyclers are sought to test the general capability of the methods to work across different time and distance scales.

All five Galilean moons of the Jovian system are of high science interest and are capable of enabling significant gravity-assisted flybys. While the target body in the idealized model is assumed to be massless, a free-return cypher connecting two massive bodies is possible as long as the flyby altitudes at the target body are sufficiently high. While the higher flyby altitudes may be less desirable in terms of science, the extra degree of freedom enabled by the inclusion of target body flybys will prove useful when transitioning to more realistic models. The five Jovian cypher systems investigated are representative of the body pairs of highest scientific interest. Europa and Io are perhaps the most scientifically attractive bodies, however Jupiter’s radiation environment prohibits long spacecraft exposure in their vicinities. Ganymede is the largest body and experiences relatively benign radiation in comparison to the closer moons. Therefore, Ganymede is chosen as the flyby body for cyclers to each of the other moons. To improve the frequency and altitudes of the Europa encounters, a Europa-Ganymede cypher is also considered. Note, the Ganymede-Callisto cyclers will experience the least radiation dose of all the Jovian cyclers.

Finally, the Saturn-Titan-Enceladus system is perhaps the best planetary moon application for the free-return cyclus theory because both moons are of high science priority and the assumptions of the idealized model are exceptionally accurate. The Titan and Enceladus orbits are nearly circular and coplanar, and Titan is capable of providing the gravity-assists as it is the largest moon in the Saturn system by several orders of magnitude. Furthermore, the small mass of Enceladus validates the massless assumption of the target body in the ideal model, thus enabling arbitrarily low flyby altitudes and excellent opportunities for science. Figure 6 illustrates how the hyperbolas at Enceladus are effectively straight lines as the mass is insufficient to significantly bend the trajectories. Low altitude flybys are therefore possible with any B -plane angle as a degree of freedom. The opportunities to begin a cyclus re-occur frequently because the synodic period of Titan and Enceladus is a very brief 1.5 days.

Table 2 reports the parameters for each relevant body. It is emphasized that the gravitational parameter of the target body (for example Enceladus in the Saturn-Titan-Enceladus system) is not required for the ideal model free return cyclus search. However, the gravity of the target body is considered when transitioning ideal model solutions to more realistic models. The patched conic ephemeris model optimization relies strictly on ephemeris files¹ for body locations and is independent of mean orbital elements. The inclinations and eccentricities are reported in Table 2 only to indicate the validity of the circular-coplanar assumptions of the idealized models. With the exception of Mercury and perhaps Mars, the circular-coplanar assumptions are reasonable for each of bodies considered. While the mean eccentricities and inclinations of the planetary moons are generally low, it is emphasized that the n -body perturbations and the oblateness effects of the primary are revealed in non-trivial perturbations to the osculating Keplerian orbital elements.

Table 2: Body Parameters

Body	Gravitational parameter (km^3/s^2)	Radius (km)	Ideal model circular orbit period (s)	Ephemeris model mean eccentricity ^a	Ephemeris model mean inclination ^a (deg)
Sun	1.3271244e11	696,000	primary	Primary	primary
Jupiter	126,686,535	71,492	primary	Primary	primary
Saturn	37,931,208	60,268	primary	Primary	primary
Mercury	22,321	2,440	7,600,552	0.206	7.00
Venus	324,860	6,052	19,414,153	0.0067	3.40
Mars	42,828.3	3,399	59,354,429	0.0933	1.85
Io	5,959.92	1,827	152,854	0.0041	0.036
Europa	3,202.74	1,561	306,822	0.0094	0.469
Ganymede	9,887.83	2,634	618,153	0.0011	0.170
Callisto	7,179.29	2,408	1,441,931	0.0074	0.187
Titan	8,978.14	2,575	1,377,684	0.0288	0.280
Enceladus	6.95	256.3	118,387	0.0047	0.009

^a <http://ssd.jpl.nasa.gov> [cited 15 Dec 2006]

All patched conic flybys referred to in this study are modeled with the assumption that they occur instantaneously and the radius of the flyby body's sphere of influence is zero. Note that other more realistic (and complicated) patched conic models exist, such as those that include hyperbolic conic propagation and sphere of influence patch point locations.

The high-fidelity force model includes the point mass gravity for the Sun, Jupiter, and Saturn. The example Titan-Enceladus cyclers include Saturn oblateness and point mass gravity for the Saturnian moons with gravitational parameters larger than $1 \text{ km}^3/\text{s}^2$. The example Ganymede-Europa cyclus includes Jupiter oblateness and point mass gravity for each of the Galilean moons. The ephemeris locations of the bodies are found from the same ephemeris files that are used for the patched conic model¹. The poles and prime meridians for Jupiter and Saturn are based on the most recent data from the IAU Working Group on Cartographic Coordinates and Rotational Elements of the Planets and Satellites [21].

¹ URL: <http://naif.jpl.nasa.gov/naif/spiceconcept.html> [cited 15 Dec 2006].

URL: ftp://naif.jpl.nasa.gov/pub/naif/generic_kernels/spk/planets/de414.bsp [cited 15 Dec 2006].

URL: ftp://naif.jpl.nasa.gov/pub/naif/generic_kernels/spk/satellites/jup230.bsp [cited Dec 15 2006]

URL: ftp://naif.jpl.nasa.gov/pub/naif/generic_kernels/spk/satellites/a_old_versions/sat242.bsp [cited 15 Dec 2006]

IDEALIZED MODEL CYCLER SEARCH

Each ideal model cycler search results in hundreds of variations of cyclers with a variety of defining characteristics. While the solution sets are too large to document here, the complete trajectories are archived for future use. A sampling of previously undocumented promising ideal model cyclers is summarized in the following figures and tables. Figure 7 and Figure 8 illustrate the trajectories for full cycles of selected promising solutions, where each cycle begins on the dot and ends on the cross and the numbers in the parenthesis of each title indicate the flyby body v_∞ in km/s and the solution ID respectively.

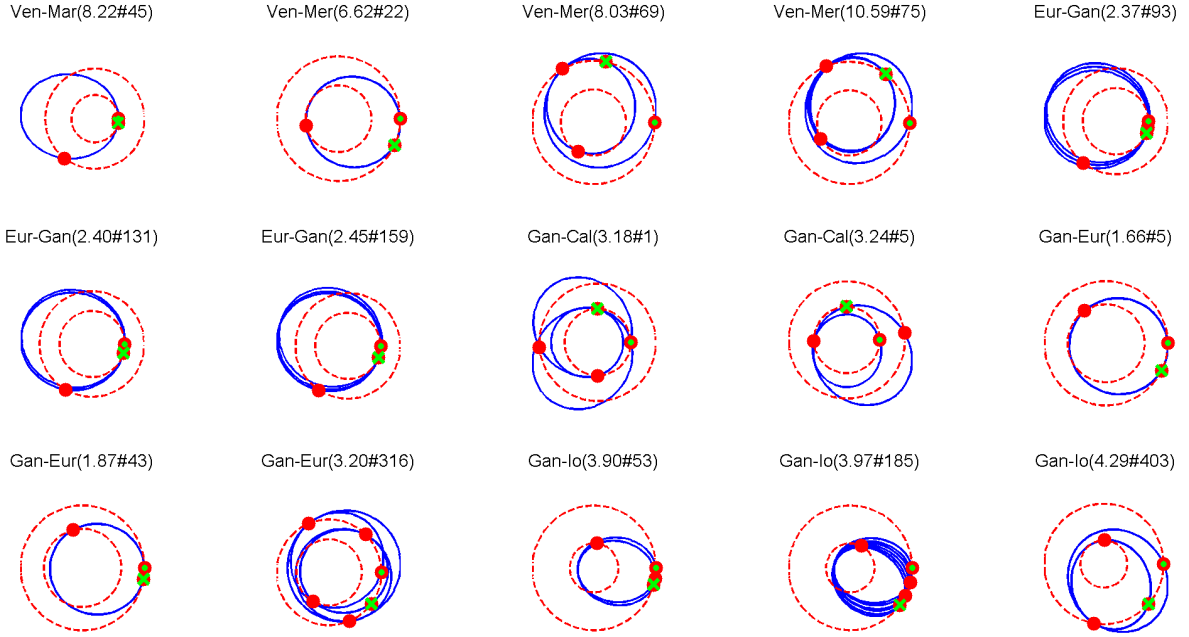


Figure 7: Representative heliocentric and Jovian ideal model ballistic cyclers

Table 3: Characteristics of promising heliocentric and Jovian ballistic ideal model cyclers

Body A	Body B	ID	Synodic period (day)	v_∞ A (km/s)	v_∞ B (km/s)	Number of legs	Period (day)	Petal period (yr)	Min flyby alt. at Body A (km)	Min dist. to primary (km)	Max dist. to primary (km)	Transit A→B (day)	Transit B→A (day)
Venus	Mars	45	333.9	8.22	12.96	1	667.8	-65.68	19,784	108,067,501	341,571,371	554.89	112.96
Venus	Mercury	22	144.6	6.62	8.61	1	433.7	-16.99	3,322	56,590,949	109,421,190	222.09	211.61
Venus	Mercury	69	144.6	8.03	10.68	2	722.8	9.13	6,111	54,928,670	125,249,833	204.09	219.07
Venus	Mercury	75	144.6	10.59	14.57	3	1,156.5	21.54	5,108	49,210,147	130,112,776	196.25	216.40
Europa	Ganymede	93	7.05	2.37	4.10	3	28.2	-1.33	1,293	670,200	1,459,911	5.68	8.42
Europa	Ganymede	131	7.05	2.40	4.10	2	21.2	-1.33	1,113	669,299	1,459,266	5.65	8.40
Europa	Ganymede	159	7.05	2.45	4.11	3	28.2	-1.33	1,261	667,983	1,459,994	5.63	8.37
Ganymede	Callisto	1	12.52	3.18	3.26	3	37.6	0.41	247	826,589	2,415,871	9.90	2.61
Ganymede	Callisto	5	12.52	3.24	3.34	2	37.6	0.41	328	821,915	2,390,844	10.14	16.67
Ganymede	Europa	5	7.05	1.66	2.57	1	35.3	-1.33	1,819	633,307	1,080,067	12.14	23.11
Ganymede	Europa	43	7.05	1.87	3.89	1	14.1	-1.33	8,861	564,558	1,072,330	6.52	7.58
Ganymede	Europa	316	7.05	3.20	3.81	4	49.4	-1.33	1,447	592,969	1,496,829	7.60	12.23
Ganymede	Io	53	2.35	3.90	9.85	2	21.2	-1.33	518	280,283	1,075,918	8.65	5.54
Ganymede	Io	185	2.35	3.97	9.90	6	49.4	-1.33	603	277,384	1,080,403	8.62	5.50
Ganymede	Io	403	2.35	4.29	4.34	2	56.4	-1.33	540	412,959	1,336,522	17.14	12.63

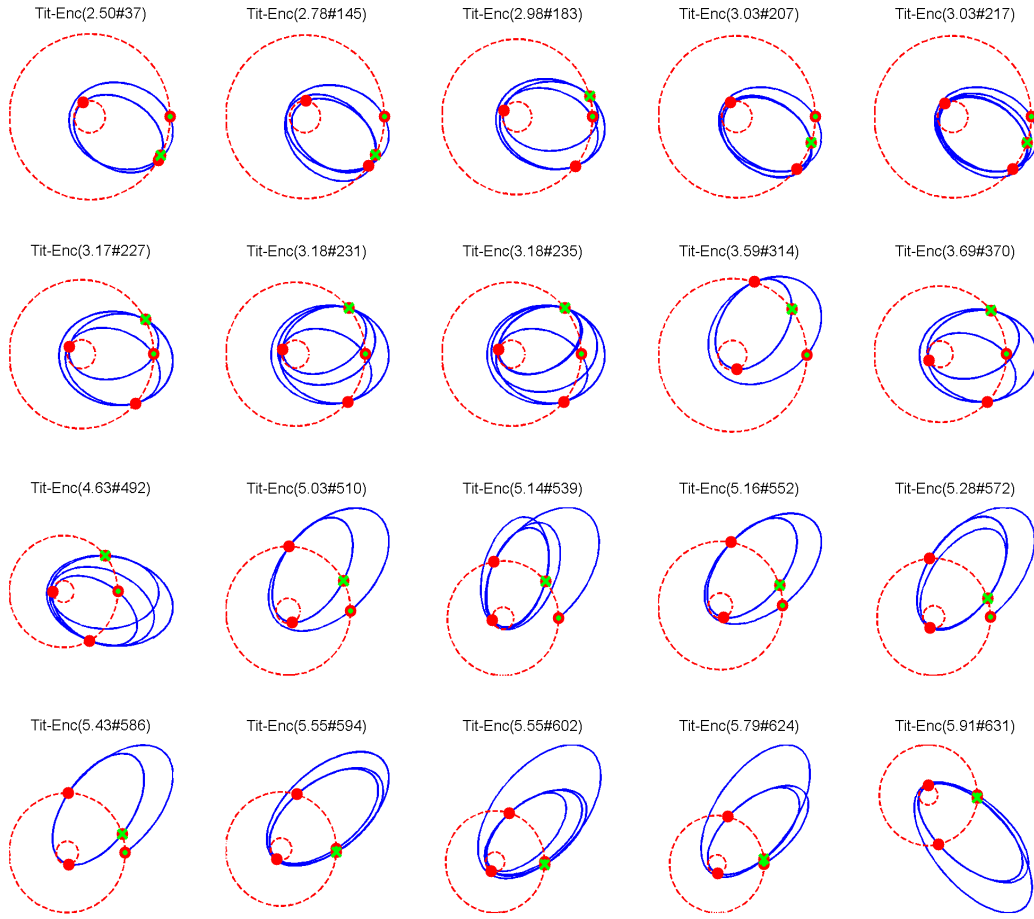


Figure 8: Representative Titan-Enceladus ideal model ballistic cyclers

Table 4: Characteristics of promising ballistic Titan-Enceladus ballistic ideal model cyclers

ID	v_{∞} T (km/s)	v_{∞} E (km/s)	Number of legs	Period (day)	Petal period (yr)	Min flyby alt. at Titan (km)	Min dist. ^a to Saturn (km)	Max dist. to Saturn (km)	Transit T→E (day)	Transit E→T (day)
37	2.50	5.17	2	94.4	-3.34	1,377	219,772	1,296,179	39.85	40.04
145	2.78	7.33	3	94.4	-3.34	1,067	185,227	1,335,036	31.94	32.23
183	2.98	4.66	3	64.5	4.16	3,304	227,827	1,441,656	10.65	5.29
207	3.03	5.08	4	63.0	-3.34	3,905	192,449	1,372,495	10.60	5.34
217	3.03	5.08	4	63.0	-3.34	10,059	192,449	1,372,495	5.17	10.78
227	3.17	5.98	3	80.9	2.90	1,183	209,397	1,555,251	10.50	5.45
231	3.18	6.04	4	97.4	2.41	2,140	208,590	1,637,907	10.49	5.46
235	3.18	6.04	5	97.4	2.41	1,843	208,590	1,637,907	10.49	5.46
314	3.59	6.88	2	49.5	1.32	1,218	196,276	1,673,806	19.52	10.77
370	3.69	4.15	3	97.4	2.41	1,343	221,429	1,798,164	21.54	26.30
492	4.63	5.61	4	97.4	2.41	4,085	220,423	2,494,396	14.67	14.49
510	5.03	7.27	2	80.9	2.90	1,852	196,399	2,531,474	15.81	29.31
539	5.14	8.08	4	97.4	2.41	1,821	183,032	2,898,708	29.36	15.84
552	5.16	7.69	2	112.4	6.06	3,784	189,939	2,431,736	30.66	30.39
572	5.28	4.69	3	112.4	6.06	1,798	201,896	2,899,479	56.37	19.99
586	5.43	6.68	2	112.4	6.06	3,874	208,262	2,899,438	73.04	19.50
594	5.55	5.76	3	127.4	-38.20	6,348	210,686	2,944,806	22.31	22.14
602	5.55	5.76	4	127.4	-38.20	1,469	168,068	3,563,396	22.31	22.14
624	5.79	7.97	3	95.9	15.77	1,961	189,020	3,606,073	22.49	22.23
631	5.91	7.49	3	127.4	-38.20	4,243	197,913	3,625,914	21.66	45.42

^a For the Titan-Enceladus cyclers, Saturn's G rings pose a hazard out to $r \sim 176,000$ km. Synodic period=1.50 days

Table 3 and Table 4 report important metrics that characterize and define each free-return cyclers solution illustrated in Figure 7 and Figure 8. The short synodic periods of the planetary moon systems lead to a large number of solutions and the multiple timing variations of each solution lead to a vast design trade space when comparing solutions for different applications. The following paragraphs discuss the important cyclers characteristics and design trades associated with each of the columns of Table 3 and Table 4.

The v_{∞} values at the flyby body and the target body are important measures of energy. Depending on the source of the cyclers spacecraft, the cost of initiating a cyclers can increase or decrease with v_{∞} . The initiation cost for an Earth-Mars cyclers increases with Earth v_{∞} because the cyclers must be initially launched from Earth [5]. On the other hand, a planetary moon cyclers will often be more expensive to initiate for lower values of flyby body v_{∞} because the cyclers spacecraft initiates from an interplanetary trajectory ending in a high speed hyperbolic approach.

To insert into a planet-centric cyclers from an interplanetary trajectory, propulsive (or perhaps aerocapture) maneuvers are required to capture around the planet and ultimately achieve the correct moon-centered v_{∞} . The rendezvous cost from the cyclers to the flyby or target body scales directly with v_{∞} . Science measurements during a flyby of either body will be directly impacted by the body centered velocities. Depending on the instruments and applications, it may be desirable to perform flybys with both large and small v_{∞} values.

The ‘Number of legs’ column in Table 3 and Table 4 indicates the number of flyby body free-return trajectories, where one of the legs includes an encounter with the target body. Thus, a cyclers with n legs has $n+1$ flybys per cycle. For science purposes, it is desirable for a cyclers to include as many flybys as possible.

The cyclers period is the combined time of flight of each leg and is constrained to be an integer multiple of the system synodic period. Because there is only one guaranteed encounter with the target body per full cycle, the cyclers period dictates the frequency of target body encounters. As [7] illustrates, the number of cyclers solutions increases dramatically as the allowable period increases. Further, the enumerating technique becomes practically infeasible when the allowable cyclers periods are too long. For reasonable computation run-times (less than a few days on one modern processor), a general rule of thumb is to seek solutions with periods less than or equal to 8 flyby body periods. This rule limits the number of potential cyclers legs to approximately 10. Less exhaustive searches such as the one described in [5] can substantially increase the number of potential legs and the cyclers period, however these solutions do not include $n\pi$ transfers when $n > 2$. To emphasize the importance of short delays between successive target body encounters, the enumerating technique based on [7] is used exclusively for the present study.

The petal periods reported in Table 3 and Table 4 are a measure of the angular difference in locations of the flyby body between consecutive cycles. If the trajectories are considered ‘petals’ on a flower that is centered at the primary, the petal period is the time required to complete the flower with 2π radians of petals. This metric is most important for the planet-centric cyclers with flyby bodies that are synchronously locked with their orbital rates. For the synchronously rotating body, the sequence of $v_{\infty -}$ and $v_{\infty +}$ vectors associated with each flyby remains unchanged in the body-fixed frame for successive periods. (The only exception is the case of a resonant flyby where there is a potential degree of freedom in choosing the placement of v_{∞} along the full-rev circle as illustrated in Figure 1.) Therefore, in the idealized model, the ground tracks of each flyby of the gravity-assist body will be identical for successive cycles. For example, if there are four flybys of the gravity-assist body during each cycle, then the set of the four ground tracks will be repeated every cycle (again with the exception of any resonant flybys with a degree of freedom). Of course, when perturbations of a realistic model are considered, the ground-tracks are expected to be quasi-periodic rather than exactly repeating as in the ideal model.

Because the periods of the planet-centric cyclers are short compared to the orbital period of the primary, the sun-line direction is approximately fixed. Consequently, the lighting conditions for science measurements during each flyby will change as the orientation of the petals rotate around the primary. The petal period is therefore the approximate time required to achieve all possible lighting conditions for each of the $n+1$ flybys on a given cyclers. For the planet-centric cyclers with synchronously rotating bodies, a short petal period is highly desirable. Note, the sign of the petal period indicates the direction of rotation.

The minimum and maximum distances to the primary may be useful for filtering cyclers that exceed a desired range of operation. The Saturn centric cyclers require a conservative minimum distance of 2.92 Saturn radii (~176,000 km) to avoid harmful ring particle collisions.

The final two columns of Table 3 and Table 4 report the transit times involving the target body. As mentioned previously, each ideal model cycler consisting of free-return trajectories to the flyby body can be initiated at multiple times such that an encounter with the target body is ensured. The transit leg trajectory will intersect the path of the target body once on an inbound path and once on an outbound path (except in the limiting case where the periapse of the transit is the radius of the target body orbit). Further, the inbound and outbound encounter opportunities are repeated for each revolution of a multiple revolution transit leg. It is emphasized that multiple pairs of transit times are possible for each cycler reported in Table 3 and Table 4, although only one pair is listed. For operational purposes it is difficult to schedule consecutive flybys within 3 or 4 days (and transit times greater than 10 days are preferable). For the fast moving systems such as the Titan-Enceladus system, a minimum transit time of 3 days is an important constraint because many of the favorable cycler solutions fail to have any transit time pairs that meet this requirement. Note that transit time pairs with near equal magnitudes will generally lead to improved convergence properties when transitioning the solution to an ephemeris model.

Table 5 and Table 6 provide the formal nomenclature associated with each or the reported ideal model cyclers. The purpose of the naming system is to provide an efficient means of describing these complicated trajectories uniquely. Given the definitions outlined in [8] and a descriptor string for each leg of an arbitrary cycler, all of its characteristics can be calculated, and the entire trajectory can be systematically reproduced. Note that each leg begins with an h, f, or g representing a half-revolution (odd $n\pi$), full-revolution (even $n\pi$), or a generic (non- $n\pi$) free-return respectively. A capital letter indicates the leg that includes the target body encounter.

Table 5: Formal nomenclature for cyclers from Table 3

ID	Leg 1	Leg 2	Leg 3	Leg 4	Leg 5	Leg 6
VenMar#45	G(2.97216,349.97729,U)	-	-	-	-	-
VenMer#22	G(1.93012,1054.84284,U)	-	-	-	-	-
VenMer#69	g(1.33364,480.11127,Ls)	G(1.88322,1037.96013,U)	-	-	-	-
VenMer#75	g(1.31055,471.79942,U)	G(1.83643,1021.11483,U)	f(2:3,74.20508,0.00960)	-	-	-
EurGan#93	g(1.97030,349.30891,U)	G(3.97176,709.83427,U)	f(2:1,88.69348,0.57296)	-	-	-
EurGan#131	G(3.95655,704.35739,U)	f(2:1,87.95239,90.00000)	-	-	-	-
EurGan#159	G(3.94206,699.14318,U)	f(2:1,87.24509,120.26932)	f(2:1,87.24509,59.73068)	-	-	-
GanCal#1	G(1.74871,269.53421,U)	g(1.50246,540.88534,L)	f(2:1,77.40130,0.03291)	-	-	-
GanCal#5	g(1.50425,541.53130,L)	G(3.74691,628.88825,U)	-	-	-	-
GanEur#5	G(4.92758,2493.92898,U)	-	-	-	-	-
GanEur#43	G(1.97103,1069.57159,U)	-	-	-	-	-
GanEur#316	g(1.31322,472.76044,U)	h(1.5,540.0,L,-3.98557)	g(1.31322,472.76044,U)	G(2.77217,1357.97970,U)	-	-
GanIo#53	g(0.97232,710.03419,U)	G(1.98423,1434.32320,U)	-	-	-	-
GanIo#185	g(0.96288,706.63724,U)	f(1:2,84.97911,89.99999)	g(0.96288,706.63724,U)	f(1:2,84.97911,57.73932)	G(1.97285,1430.22609,U)	f(1:2,84.97911,90.00890)
GanIo#403	g(3.72334,1700.40403,L)	G(4.16078,2217.88234,L)	-	-	-	-

Table 6: Formal nomenclature for cyclers from Table 4

ID	Leg 1	Leg 2	Leg 3	Leg 4	Leg 5
TitEnc#37	g(0.91247,688.48877,U)	G(5.01017,3963.66276,L)	-	-	-
TitEnc#145	g(0.89794,683.25735,U)	G(4.02471,3248.89419,L)	f(1:2,64.90258,142.00153)	-	-
TitEnc#183	g(0.89055,680.59930,U)	g(2.15189,1134.67873,U)	F(1:2,61.35060,180.0)	-	-
TitEnc#207	g(0.88869,679.92726,U)	g(1.05974,741.50710,L)	F(1:2,60.31038,180.0)	f(1:2,60.31038,167.71581)	-
TitEnc#217	g(0.88869,679.92726,U)	F(1:2,60.31038,0.0)	g(1.05974,741.50710,L)	f(1:2,60.31038,-179.90781)	-
TitEnc#227	g(0.88489,678.56001,U)	g(3.19166,1508.99845,U)	F(1:2,57.91040,180.0)	-	-
TitEnc#231	g(0.88468,678.48383,U)	g(1.22599,441.35506,U)	f(3:5,55.34820,167.71581)	F(1:2,57.76202,180.0)	-
TitEnc#235	g(0.88468,678.48383,U)	g(1.22599,441.35506,U)	f(2:3,55.18988,179.99996)	F(1:2,57.76202,180.0)	f(1:2,57.76202,154.65857)
TitEnc#314	g(1.20284,433.02184,U)	G(1.89950,1403.81944,Ls)	-	-	-
TitEnc#370	g(0.87690,675.68567,Ls)	g(2.23376,804.15321,U)	F(3:5,48.53243,180.0)	-	-
TitEnc#492	G(1.82913,1018.48816,L)	f(1:1,40.91079,0.00006)	g(2.28153,461.35072,U)	f(1:1,40.91079,179.99987)	-
TitEnc#510	g(2.24732,449.03519,U)	G(2.82923,1378.52326,L)	-	-	-
TitEnc#539	g(1.27588,99.31575,U)	f(1:1,35.08563,179.99992)	G(2.83479,1380.52313,L)	f(1:1,35.08563,-0.00001)	-
TitEnc#552	g(3.22220,799.99089,U)	G(3.82857,1738.28475,L)	-	-	-
TitEnc#572	g(1.26162,94.18203,U)	G(4.78915,1724.09360,L)	f(1:1,33.41047,-0.00438)	-	-
TitEnc#586	g(1.24728,89.02223,U)	G(5.80348,2089.25340,L)	-	-	-
TitEnc#594	g(2.20335,433.20509,U)	G(2.78752,1003.50729,L)	f(3:2,34.01307,0.00040)	-	-
TitEnc#602	g(2.20335,433.20509,U)	f(1:1,30.24411,-176.67648)	G(2.78752,1003.50729,L)	f(2:1,36.04284,0.00001)	-
TitEnc#624	g(1.21211,76.36107,U)	G(2.80454,1009.63414,L)	f(2:1,33.39447,-0.01457)	-	-
TitEnc#631	g(1.78380,642.16785,L)	G(4.20707,794.54453,U)	f(2:1,32.10391,179.99994)	-	-

PATCHED CONIC EPHEMERIS MODEL OPTIMIZATION

Multiple cycles of a few example cyclers are transitioned to the patched conic ephemeris model and illustrated in Figure 9 - Figure 13. Remarkably, many of the cyclers remain ballistic. The Venus-Mars #45 solution in Figure 9(a) easily converges to ballistic and is similar to the Earth-Mars Aldrin cycler [3,13] because it consists of just one multiple revolution non-resonant return. Despite several promising Venus-Mercury ideal model cyclers such as #22 and #45 presented in Figure 7, no ephemeris solutions are presented because the large eccentricity of Mercury proved to high for multiple cycles to remain ballistic in the ephemeris model. The Ganymede-Callisto #1 solution from Figure 9(b) is a representative ballistic solution that enjoys very low radiation exposures and an extremely short petal period (~ 0.41 years from Table 3) as indicated by the completion of ~ 2.5 rotations around Jupiter over the course of 10 cycles. The Ganymede-Europa #316 ballistic solution from Figure 10(a) is noteworthy because of its many legs, the large out-of-plane motion, and the inclusion of a 3π transfer[†] (2^{nd} leg from Table 5). The Europa-Ganymede #131 solution from Figure 10(b) is a relatively simple cycler that enables 2 Europa flybys and 1 Ganymede flyby every 21 days, and the radiation exposure is minimized because it never goes inside of Europa's orbit.

Figure 11 - Figure 13 give examples of Titan-Enceladus patched conic ephemeris cyclers. Of the low v_{∞} solutions, #235 from Figure 12(b) is particularly promising. This example includes 45 Titan flybys, 9 Enceladus flybys, and a flight time of 2.4 years. The Enceladus encounters are equally spaced around Saturn enabling the full possibilities of lighting conditions, and the trajectory easily converges to ballistic due to the large flyby altitudes in the ideal model solution. Further, as is common for all planetary cyclers, initiation opportunities are abundant because of the short synodic period (1.5 days for Titan-Enceladus system).

Note that all the free-return cyclers are guaranteed to have exactly one target-body encounter per cycle. However, the fast Enceladus period leads to the possibility for many untargeted flybys, especially when the transit leg includes multiple revolutions. Close inspection of the Cycler#235 in Figure 12(b) shows 24 additional encounters with close approaches less than 200,000 km while 4 of those are less than 100,000 km. As a second

[†] The odd- $n\pi$ solutions are sought in all of the ideal model cycler searches in this study. However, unlike the Earth-Mars case [7], ballistic solutions that include odd- $n\pi$ free returns are much less common for the planet-centered cyclers considered.

example, the transit leg on the #37 cyclers from Figure 11(a) is an 11+ revolution transfer. Thus, in addition to the 8 targeted Enceladus flybys, there are 17 untargeted Enceladus flybys with close approaches less than 100,000 km where 9 of those are less than 25,000 km. The frequency and proximity of the untargeted flybys are highly sensitive to a specific epoch.

Table 7 gives the pertinent data for the example patched conic ephemeris model Cyclers#235 shown in Figure 12(b). While the Titan-Enceladus system is circular coplanar to first order, a quick comparison between the times and v_∞ values of Table 7 and Table 4 illustrates the non-trivial effects of using an ephemeris vs. a circular coplanar model.

The v_∞ at Titan for the Cassini spacecraft has spanned the approximate range of 5.8 \rightarrow 6.0 km/s. Considering that small leveraging maneuvers near apoapse [16] can significantly reduce flyby body v_∞ , the ideal model Titan-Enceladus cyclers with $v_\infty > \sim 5$ km/s (see Table 4) are reasonable for extended mission consideration. Of the high energy cyclers, those in Figure 13 are illustrated because of their short petal periods leading to favorable rotation rates around Saturn. The out of plane component of solution #572 from Figure 13(a) is also attractive; however, as the title indicates, this 562 day trajectory requires 222 m/s Δv and fails to remain outside of Saturn's G ring radius of 176,000 km. The #586 trajectory from Figure 13(b) remains outside the G ring and requires 154 m/s to achieve 5 Enceladus and 10 Titan encounters in 561 days. Because the higher v_∞ trajectories are dynamically more constrained, the patched conic ephemeris optimization outlined in [9] converges to ballistic solutions much easier for trajectories with low v_∞ . Noting that the method in [9] has only a limited ability to minimize Δv for non-ballistic trajectories, it is anticipated that detailed optimization of any one trajectory with a high-fidelity optimizer will reduce Δv requirements.

Venus-Mars, ID#45, 10 cycles in ephemeris model, 10 V. & 10 M. flybys
 start=7-19-2011, TOF=6675.9 days, $\Delta v_{TOTAL}=0$ m/s, $r_{MIN}=1.07e+008$ km

Ganymede-Callisto, ID#1, 10 cycles in ephemeris model, 30 G. & 10 C. flybys
 start=9-27-2013, TOF=375.7 days, $\Delta v_{TOTAL}=0$ m/s, $r_{MIN}=8.14e+005$ km

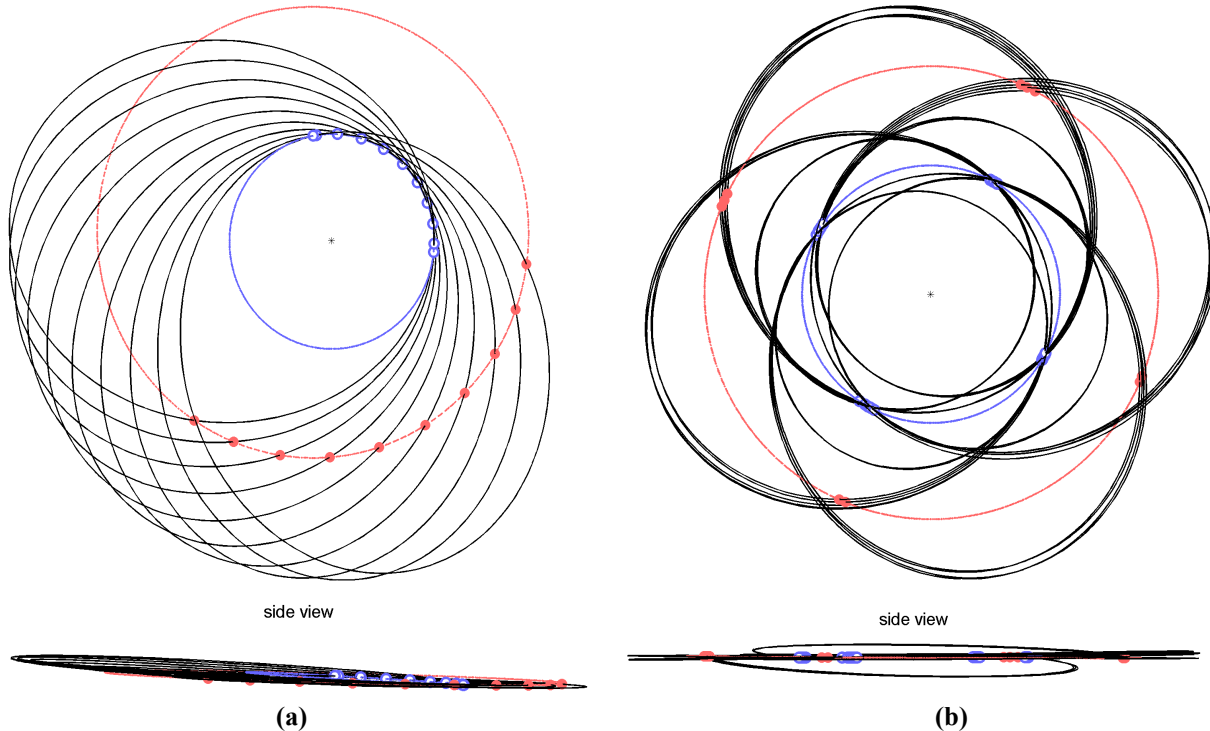


Figure 9: Example Venus-Mars and Ganymede-Callisto ephemeris patched conic cyclers

Ganymede-Europa, ID#316, 10 cycles in ephemeris model, 40 G. & 10 E. flybys
 start=4-24-2019, TOF=493.5 days, $\Delta v_{TOTAL}=0$ m/s, $r_{MIN}=5.91e+005$ km

Europa-Ganymede, ID#131, 10 cycles in ephemeris model, 20 E. & 10 G. flybys
 start=4-23-2019, TOF=211.8 days, $\Delta v_{TOTAL}=61$ m/s, $r_{MIN}=6.6e+005$ km

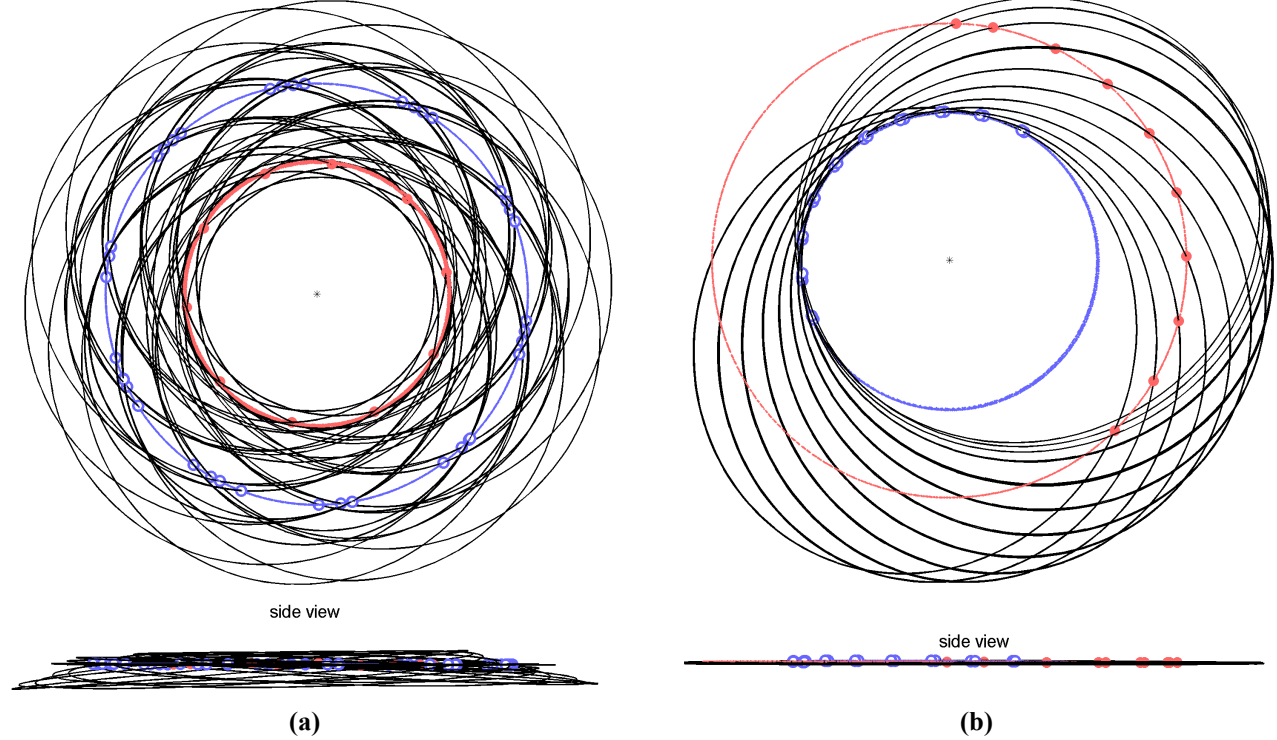


Figure 10: Example Ganymede-Europa and Europa-Ganymede ephemeris patched conic cyclers

Titan-Enceladus, ID#37, 8 cycles in ephemeris model, 16 T. & 8 E. flybys
 start=1-14-2024, TOF=756.2 days, $\Delta v_{TOTAL}=131$ m/s, $r_{MIN}=1.83e+005$ km

Titan-Enceladus, ID#183, 10 cycles in ephemeris model, 30 T. & 10 E. flybys
 start=1-18-2024, TOF=644.5 days, $\Delta v_{TOTAL}=0$ m/s, $r_{MIN}=202688$ km

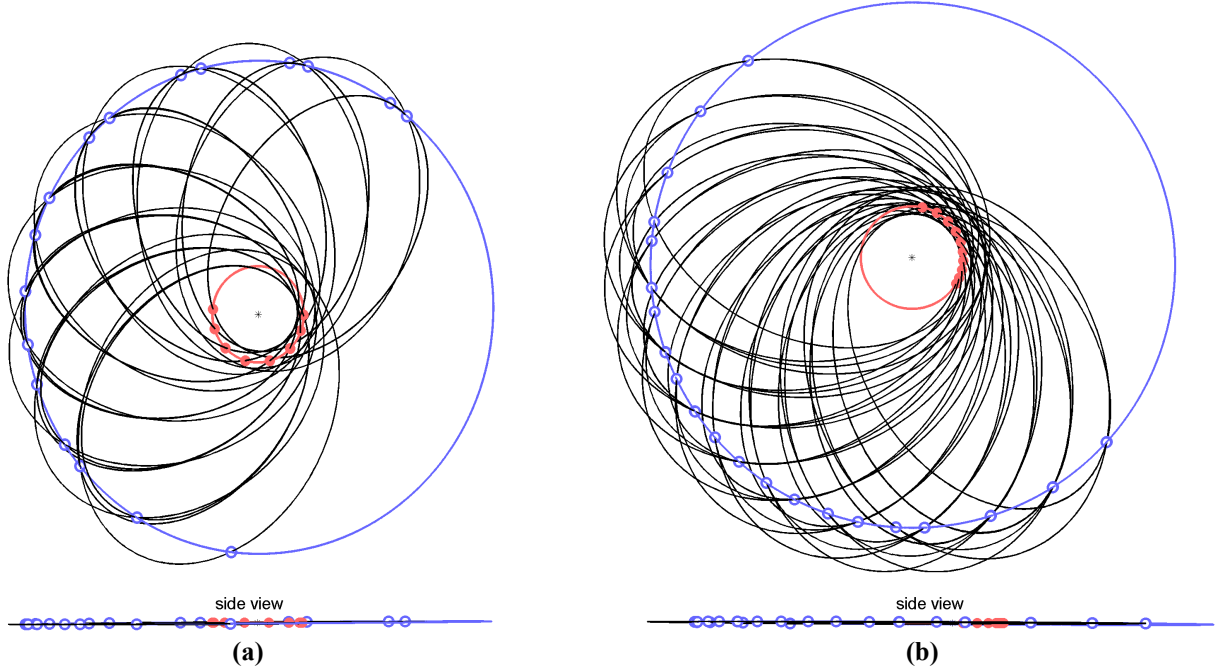


Figure 11: Example low v_{∞} Titan-Enceladus ephemeris patched conic cyclers, Part I

Titan-Enceladus, ID#207, 10 cycles in ephemeris model, 40 T. & 10 E. flybys
 start=1-17-2024, TOF=629.5 days, $\Delta v_{TOTAL}=28$ m/s, $r_{MIN}=1.73e+005$ km

Titan-Enceladus, ID#235, 9 cycles in ephemeris model, 45 T. & 9 E. flybys
 start=1-9-2024, TOF=876.9 days, $\Delta v_{TOTAL}=1$ m/s, $r_{MIN}=185692$ km

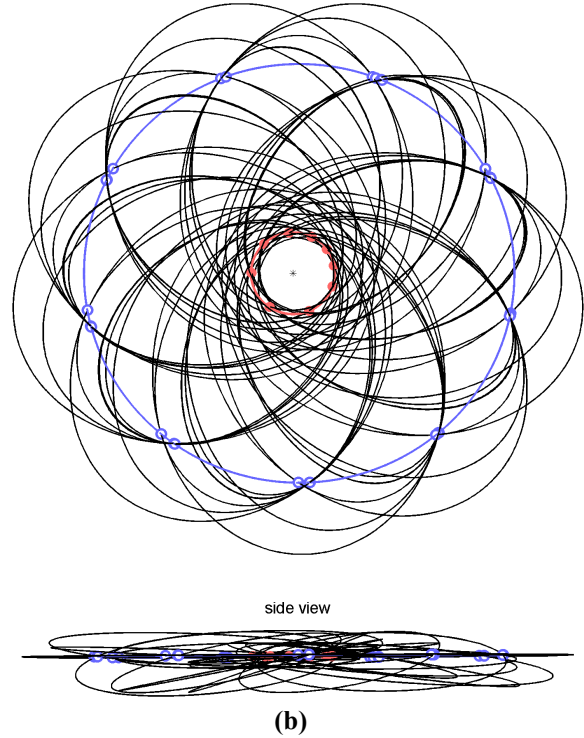
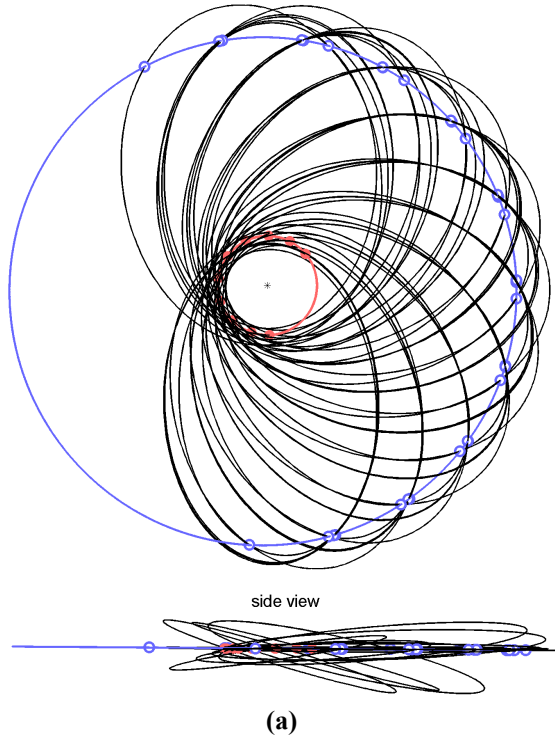


Figure 12: Example low v_{∞} Titan-Enceladus ephemeris patched conic cyclers, Part II

Titan-Enceladus, ID#572, 5 cycles in ephemeris model, 15 T. & 5 E. flybys
 start=1-17-2024, TOF=562 days, $\Delta v_{TOTAL}=222$ m/s, $r_{MIN}=1.66e+005$ km

Titan-Enceladus, ID#586, 5 cycles in ephemeris model, 10 T. & 5 E. flybys
 start=1-10-2024, TOF=561.5 days, $\Delta v_{TOTAL}=154$ m/s, $r_{MIN}=182928$ km

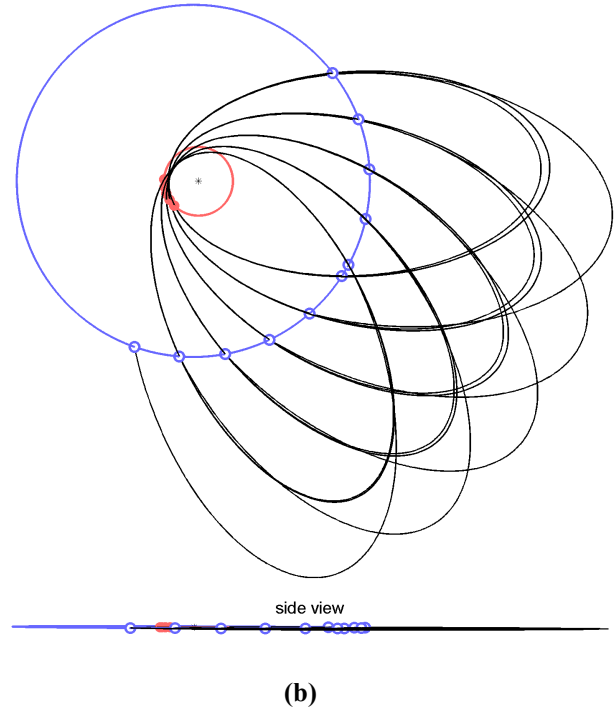
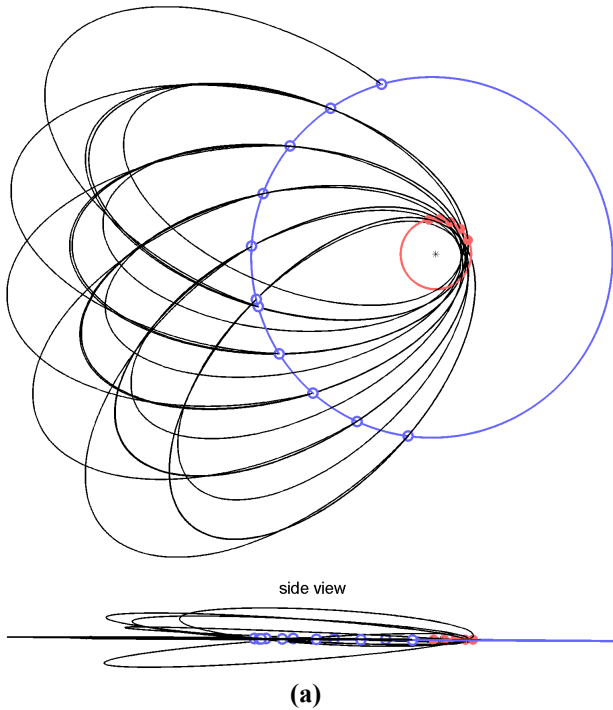


Figure 13: Example high v_{∞} Titan-Enceladus ephemeris patched conic cyclers (applicable to Cassini extended missions)

Table 7: Details^a on the patched conic ephemeris Titan-Enceladus Cyclers#235 from Figure 12(b)

Leg #	Start (T or E)	TOF (day)	v_{∞} (km/s)	RA (deg)	DEC (deg)	Leg #	Start (T or E)	TOF (day)	v_{∞} (km/s)	RA (deg)	DEC (deg)
1	T	14.187	3.103	105.17	-25.25	28	T	10.507	3.246	-43.35	15.75
2	T	19.570	3.145	170.61	0.81	29	E	5.444	5.951	-6.82	-3.17
3	T	31.891	3.115	137.84	-20.69	30	T	15.946	3.257	-32.21	29.65
4	T	10.459	3.114	153.69	-8.13	31	T	14.063	3.257	-51.66	18.92
5	E	5.489	5.506	-174.11	10.05	32	T	19.509	3.206	9.19	-10.24
6	T	15.945	3.120	155.95	-12.06	33	T	31.891	3.239	-23.19	11.67
7	T	14.118	3.120	146.02	-11.62	34	T	10.539	3.239	-8.05	-1.28
8	T	19.600	3.172	-152.35	18.14	35	E	5.403	6.901	26.67	-18.86
9	T	31.891	3.145	178.52	-6.37	36	T	15.945	3.229	3.55	12.02
10	T	10.458	3.145	-169.54	10.17	37	T	14.130	3.229	-15.92	2.62
11	E	5.494	4.499	-135.54	25.54	38	T	19.484	3.178	47.86	-24.19
12	T	15.945	3.162	-166.67	4.98	39	T	31.891	3.205	11.06	-5.46
13	T	14.051	3.162	-177.16	7.13	40	T	10.554	3.205	27.66	-17.78
14	T	19.607	3.200	-109.57	27.44	41	E	5.382	7.423	64.74	-27.85
15	T	31.891	3.187	-144.72	10.96	42	T	15.945	3.186	37.34	-3.58
16	T	10.481	3.187	-129.14	24.24	43	T	14.189	3.186	18.96	-14.66
17	E	5.473	4.185 ^b	-90.73	28.61	44	T	19.483	3.158	91.48	-27.16
18	T	15.946	3.211	-129.89	43.74	45	T	31.891	3.164	50.27	-13.39
19	T	14.014	3.211	-137.83	22.79	46	T	10.540	3.164	68.81	-26.96
20	T	19.590	3.216	-65.03	23.05	47	E	5.394	7.380	107.11	-25.37
21	T	31.891	3.223	-104.96	24.03	48	T	15.945	3.142	71.05	-17.91
22	T	10.485	3.223	-84.26	26.48	49	T	14.212	3.142	58.94	-26.25
23	E	5.471	4.851	-43.15	15.31	50	T	19.510	3.150	132.82	-17.26
24	T	15.946	3.250	-77.08	42.78	51	T	31.891	3.133	90.55	-15.82
25	T	14.018	3.250	-93.47	27.51	52	T	10.506	3.133	112.37	-23.47
26	T	19.550	3.221	-26.26	7.91	53	E	5.428	6.740	147.10	-10.89
27	T	31.891	3.246	-56.82	33.89	54	T	15.945	3.110	111.26	-13.18

^a The propagation is a zero radius sphere of influence patched conic and the ephemeris positions of the moons are relative to a fixed Saturn. Right ascension (RA) and declination (DEC) are expressed in the ecliptic J2000 frame. The start date is 8774.549 days after J2000 (Jan-10-2024).

^b For orbiting or landing at Enceladus, a mission designer should target the lowest v_{∞} of all the Enceladus encounters. Note the minimum possible in the ideal model is from the Hohmann transfer: Enceladus $v_{\infty}=3.71$ km/s, Titan $v_{\infty}=2.39$ km/s

HIGH-FIDELITY OPTIMIZATION

The assumptions of the zero radius sphere of influence patched conic ephemeris model include several non-trivial error sources that manifest when transitioning solutions to a high-fidelity model. These error sources include the non-zero radius of the sphere of influence, central-body oblateness, and n -body perturbations. For the examples considered in this study, the largest of these error sources is the assumption that the sphere of influence for the flyby body is negligible compared to the size of the flyby orbit around the primary. A common definition for the radius of the sphere of influence around a small body in a circular orbit around a primary is given in Eq. (10) where d is the separation distance between the bodies and μ is the mass ratio of the smaller body to the primary [22].

$$r_{SOI} = d \mu^{2/5} \quad (10)$$

The patched conic assumption is clearly better in the case of the heliocentric cyclers noting that $r_{SOI} \sim 0.006d$ for the Sun-Venus and the Sun-Earth systems compared to $\sim 0.035d$ for the Saturn-Titan system, $\sim 0.023d$ for the Jupiter-Ganymede system, and $\sim 0.014d$ for the Jupiter-Europa system. Further, the oblateness effects of the primary and n -body perturbations (both of which are ignored in our patched conic ephemeris model) play a significantly greater role in the planet-centric cyclers. For these reasons the transition to a high-fidelity force model is substantially more difficult for the planet-centric cyclers. To demonstrate the transition, Table 8 summarizes the results of optimized single cycles of four example cyclers in high-fidelity models using the patched conic ephemeris solutions as initial guesses.

Table 8: Single cycles optimized in high-fidelity models^{1,2,3}

(a) Titan-Enceladus #183			(b) Titan-Enceladus #235			(c) Titan-Enceladus #586			(d) Ganymede-Europa #316		
Encounter	t (day)	flyby alt. (km) or Δv	Encounter	t (day)	flyby alt. (km) or Δv	Encounter	t (day)	flyby alt. (km) or Δv	Encounter	t (day)	flyby alt. (km) or Δv
Titan	0.00	10,510	Titan	0.00	1,858	Titan	0.00	4,417	Ganymede	0.00	1,224
Dione	7.13	2,879	Δv	8.95	1.1 m/s	Tethys	1.51	11,656	Δv	8.78	78.7 m/s
Dione	7.36	79,911	Rhea	9.27	49,765	Enceladus	1.58	82,145	Ganymede	10.80	2,094
Mimas	7.45	166,523	Δv	13.55	13.2 m/s	Dione	19.15	70,850	Ganymede	20.17	4,778
Rhea	16.63	47,197	Titan	19.58	2,040	Enceladus	19.33	154,979	Δv	23.31	42.4 m/s
Mimas	27.26	176,755	Dione	22.08	115,461	Rhea	19.99	578	Europa	27.72	495
Δv	27.29	8.8 m/s	Enceladus	22.30	145,151	Enceladus	37.13	180,599	Ganymede	39.99	8,230
Enceladus	27.36	169,665	Tethys	22.32	91,913	Dione	54.75	58,404	Ganymede	49.35	1,492
Rhea	27.72	7,541	Δv	23.30	7.5 m/s	Enceladus	54.94	184,774			
Titan	34.36	3,670	Rhea	33.38	70,927	Δv	54.98	6.5 m/s			
Δv	37.10	1.4 m/s	Titan	51.49	1,000	Tethys	55.27	106,293			
Enceladus	37.18	151,288	Enceladus	54.19	172,350	Enceladus	72.92	912			
Mimas	44.96	129,365	Enceladus	61.92	3	Δv	73.08	1.6 m/s			
Enceladus	45.02	3	Mimas	62.00	145,679	Dione	90.97	182,699			
Mimas	45.12	87,092	Tethys	62.07	76,144	Δv	91.00	3.2 m/s			
Titan	50.27	9,234	Mimas	62.24	155,684	Enceladus	91.16	4			
Rhea	52.45	113,199	Δv	63.55	20.0 m/s	Tethys	91.22	191,625			
Tethys	53.21	48,754	Titan	67.44	1,801	Titan	92.81	4,889			
Dione	61.52	148,847	Enceladus	70.13	114,438	Titan	112.30	5,693			
Δv	61.90	22.2 m/s	Enceladus	70.39	165,493						
Titan	64.45	10,201	Δv	70.45	21.1 m/s						
			Hyperion	74.79	81,157						
			Mimas	78.17	62,970						
			Titan	83.39	999						
			Δv	94.70	0.2 m/s						
			Enceladus	94.78	93,155						
			Enceladus	95.03	127,658						
			Titan	97.47	2,232						

¹ Begin date for (a) - (d) is February 1, 2024 3:23:12; January 24, 2024 3:59:16; January 29, 2024 15:24:38; and May 3, 2019 12:17:26 respectively

² Total Δv for (a) - (d) is 32, 63, 11, and 121 m/s respectively

³ The bold encounters result from the ideal model cyclers geometry while the others are serendipitous and initially untargeted.

Close approaches with flyby radii less than 200,000 km to all moons with gravitational parameters larger than $1 \text{ km}^3/\text{s}^2$ are reported in Table 8. Note that only one low altitude targeted flyby of Enceladus or Europa results from the initial guess. However, several high altitude serendipitous encounters with Enceladus occur in each of the cases (a)–(c). In particular, note that case (c) includes an extra very low altitude Enceladus encounter with a flyby altitude of 4 km. The case (a) Titan-Enceladus Cyclers#183 includes one very low altitude (3 km) and two high altitude Enceladus flybys; four medium altitude Titan encounters; and many untargeted moon encounters costing a total Δv of 32 m/s. The case (b) Titan-Enceladus Cyclers#235 includes six low altitude Titan, one low altitude Enceladus, 6 high altitude Enceladus, and many untargeted moon encounters costing a total Δv of 63 m/s. Note that a second independently optimized cycle of Titan-Enceladus Cyclers#235 required a total Δv of 40 m/s. The case (c) Titan-Enceladus Cyclers#586 includes three medium altitude Titan, two low altitude Enceladus, 4 high altitude Enceladus, and many untargeted moon encounters costing a total Δv of 11 m/s. Note the v_∞ at Titan is $\sim 5.75 \text{ km/s}$ making this example applicable for a Cassini extended mission. The case (d) Ganymede-Europa Cyclers#316 includes five targeted Ganymede, one targeted Europa, and no untargeted moon encounters costing a total Δv of 121 m/s. While not documented in Table 8, a high-fidelity simulation of one cycle of the Europa-Ganymede Cyclers#131 costs a total Δv of 58 m/s and includes an extra close flyby of Europa.

As anticipated, the patched conic ephemeris solutions with the very high flyby radii are generally more difficult to converge to the low Δv solutions in the high-fidelity models because of the large violation of the zero radius sphere of influence assumption. Future work includes seeking methods to mitigate this effect such as altering the constants in the lower-fidelity models in order to mimic for the more realistic timing and geometry in the high-fidelity model. In addition, improved ideal model (circular-coplanar) cyclers could be sought by removing the massless assumption of the target body. The Jovian system cyclers in particular would benefit from such a change.

The design of high-fidelity moon tours is generally a time consuming process involving an artistic combination of methods, software, and intuition. The examples included here are meant to demonstrate the feasibility of realistic planetary moon cyclers. Detailed refinement of each reported sequence would likely lead to improved Δv costs. Further, it is emphasized that the boundary conditions on each sequence are heavily constrained so that the timing and geometry of the cycler is maintained. Relaxing these constraints is another source that can reduce Δv costs. As an example, by adding one extra Titan leg and re-optimizing the sequence presented in Table 8(a), the total Δv reduces from 32 to 17 m/s. This dramatic improvement is not indicative of all cases. However, large maneuvers near the end of a sequence can often be significantly reduced by including additional flybys. In general, patching together and optimizing multiple cycles such as the 54 leg cycler illustrated in Table 7 and Figure 12(b) is beyond the scope of the software and intent of the present study. Future work includes automating methods to enable such multi-cycle optimization in the high-fidelity models.

CONCLUSIONS

Existing cycler search algorithms previously applied to the Earth-Mars case are generalized and improved for application to the planetary moon cycler problem. The short synodic periods of the planetary moon systems significantly widens the design space for finding useful cycler trajectories. As a result, the existence of hundreds of ideal model ballistic cyclers is demonstrated for the Galilean moon pairs at Jupiter and the Titan-Enceladus moon pair at Saturn with repeat times ranging from ~ 2 to ~ 18 weeks. The complete database is archived and can be queried or sorted for quick assessment of the cycler architecture and preliminary guesses for future planetary moon mission and tour design applications.

For evaluation in a more realistic model, an improved homotopy method is implemented that seeks multiple cycles of ballistic solutions in a patched conic ephemeris model. Notably many of the multi-cycle trajectories that include up to 54 flybys remain ballistic and several resulting examples are documented. As a feasibility demonstration, we optimize single cycles of four representative cyclers in a high-fidelity force model based on initial guesses from the patched conic ephemeris model. The preliminary analysis suggests that the high-fidelity force models often differ significantly from the zero radius sphere of influence patched conic ephemeris model for the planetary moon systems considered. However, for the Titan-Enceladus high-fidelity examples, we find that the Δv costs per flyby are similar in magnitude to Cassini, noting that the solutions are heavily epoch dependent and further refinement would likely improve the results. Future work is required to further assess the viability and strategies of designing realistic cyclers.

Special attention is paid to the Titan-Enceladus system because of the recent heightened science interest due to Cassini and the exceptional accuracy of the massless Enceladus assumption. Of the low-energy Titan-Enceladus cyclers, #235 is recommended as one of the most promising because of its short period, frequent encounters with both bodies, multiple degrees of freedom and flyby geometries at Titan, potential for full lighting conditions, and low approach velocities at Enceladus. The high energy Titan-Enceladus cyclers are candidates for the Cassini extended missions that undoubtedly will require frequent, low-cost encounters with Enceladus.

The generalized free-return cycler theory provides alternative and complementary methods to explore some of the highest priority celestial bodies according to the planetary science community including Titan, Enceladus, and the Galilean moons at Jupiter. The repeat flybys of a cycler enable remote sensing surface science as well as in situ measurements of atmospheres, electromagnetic fields, and plumes. The planetary cycler trajectories can act as stand-alone flyby missions or as roadmaps of the trade space for the traditional planetary tour design problem. Furthermore, a cycler can provide invaluable reconnaissance and act as a telecommunications relay for surface landers, orbiters, or aerial vehicles. For a very low propellant cost and only a modest percentage increase in total mission duration, the cycler architecture is an attractive option for maximizing science for a variety of planetary moon missions.

ACKNOWLEDGEMENTS

The authors thank Kim Reh, Tom Spilker, Jim Cutts, and Brent Buffington for their interest and support. Part of this work was carried out at the Jet Propulsion Laboratory, California Institute of Technology, under a contract with the National Aeronautics and Space Administration.

REFERENCES

- ¹ Rall, C. S., "Freefall Periodic Orbits Connecting Earth and Mars," Ph.D. Thesis, Department of Aeronautics and Astronautics, Massachusetts Institute of Technology, Oct. 1969.
- ² Hollister, W. M., "Periodic Orbits for Interplanetary Flight," *Journal of Spacecraft and Rockets*, Vol. 6, No. 4, 1969, pp. 366-369.
- ³ Byrnes, Dennis V., Longuski, James M., Aldrin, Buzz, "Cycler Orbit Between Earth and Mars," *Journal of Spacecraft and Rockets*, Vol. 30, No. 3, May-June 1993, pp. 334-336.
- ⁴ Nock, T., Duke, M., King, R., Jacobs, M., Johnson, L., McDonald, A., Penzo, P., Rauwolf, J., Wyszowski, C., "An Interplanetary Rapid Transit System Between Earth and Mars," *Expanding the Frontiers of Space; Space Technology and Applications International Forum – STAIF 2003*, edited by El-Genk, M. S., Melville, NY, American Institute of Physics, 2003, pp. 1074-1086.
- ⁵ Russell, R. P., Ocampo, C. A., "Systematic Method for Constructing Earth-Mars Cyclers Using Free-Return Trajectories," *Journal of Guidance, Control, and Dynamics*, Vol. 27, No. 3, 2004, pp. 321-335.
- ⁶ Russell, R. P., Ocampo, C. A., "Geometric Analysis of Free-Return Trajectories Following a Gravity-Assisted Flyby", *Journal of Spacecraft and Rockets*, Vol. 42, No. 1, 2005, pp. 694-698.
- ⁷ Russell, R. P., Ocampo, C. A., "Global Search for Idealized Free-Return Earth-Mars Cyclers," *Journal of Guidance, Control, and Dynamics*, Vol. 28, No. 2, 2005, pp. 194-208.
- ⁸ McConaghy, T. T., Russell, R. P., Longuski, J. M., "Towards a Standard Nomenclature for Earth-Mars Cycler Trajectories," *Journal of Spacecraft and Rockets*, Vol. 42, No. 4, 2005, pp. 694-698.
- ⁹ Russell, R. P., Ocampo, C. A., "Optimization of a Broad Class of Ephemeris Model Earth-Mars Cyclers," *Journal of Guidance, Control, and Dynamics*, Vol. 29, No. 2, 2006, pp. 354-367.
- ¹⁰ McConaghy, T. T., Yam, C. H., Landau, D. F., Longuski, J. M., "Two-Synodic-Period Earth-Mars Cyclers with Intermediate Earth Encounter," AAS Paper 03-509, Aug. 2003.
- ¹¹ Byrnes, D. V., McConaghy, T. T., Longuski, J. M., "Analysis of Various Two Synodic Period Earth-Mars Cycler Trajectories," AIAA Paper 2002-4423, Aug. 2002.
- ¹² Niehoff, J., "Pathways to Mars: New Trajectory Opportunities," American Astronautical Society, AAS Paper 86-172, July 1986.
- ¹³ Chen, K., McConaghy, T., Okutsu, M., Longuski, J. "A Low-Thrust Version of the Aldrin Cycler," AIAA Paper 2002-4421, Aug. 2002.
- ¹⁴ Landau, D. F., Longuski, J. M., "Guidance Strategy for Hyperbolic Rendezvous," Paper AIAA-2006-6299, Aug. 2006.
- ¹⁵ Whiffen, G. J., Sims, J. A., "Application of the SDC optimal control algorithm to low-thrust escape and capture trajectory optimization", Paper AAS 02-208, AAS/AIAA Space Flight Mechanics Meeting, San Antonio, Texas, 2002.
- ¹⁶ Strange, N.J., Sims, J.A., "Methods for the Design of V-Infinity Leveraging Maneuvers," Paper AAS 01-437, Aug. 2001.
- ¹⁷ Prussing, J. E., Conway, B. A., *Orbital Mechanics*, Oxford University Press, New York, 1993. pp.63-80.
- ¹⁸ Prussing, J. E., "A Class of Optimal Two-Impulse Rendezvous Using Multiple-Revolution Lambert Solutions," *Journal of the Astronautical Sciences*, Vol. 48, Nos. 2 and 3, April-September 2000, pp. 131-148.
- ¹⁹ Shen, H., and Tsiotras, P., "Using Battin's Method to Obtain Multiple-Revolution Lambert's Solutions," AAS Paper 03-568, Aug. 2003.
- ²⁰ Turner, A., "Low Road to Mars: The Venus-Mars Cycler," Paper AAS 07-175, Jan. 2007.
- ²¹ Seidelmann, P.K., Abalakin, V.K., Bursa, M., Davies, M.E., Bergh, C. de, Lieske, J.H., Oberst, J., Simon, J.L., Standish, E.M., Stooke, P., Thomas, P.C., "Report of the IAU/IAG Working Group on Cartographic Coordinates and Rotational Elements of the Planets and Satellites: 2000," *Celestial Mechanics and Dynamical Astronomy*, Vol. 82, Issue 1, 2002, pp. 83-111.
- ²² Wiesel, W. E., *Spaceflight Dynamics*, McGraw-Hill, Boston, 1997. pg. 300.